



NLR TP 96323

A robust multi-block Navier-Stokes flow solver for industrial applications.

J.C. Kok, J.W. Boerstoel, A. Kassies, S.P. Spekreijse

A Robust Multi-Block Navier-Stokes Flow Solver for Industrial Applications

J.C. Kok¹, J.W. Boerstoel, A. Kassies, S.P. Spekreijse

Abstract. This paper presents a robust multi-block flow solver for the thin-layer Reynolds-averaged Navier-Stokes equations, that is currently being used for industrial applications. A modification of a matrix dissipation scheme has been developed, that improves the numerical accuracy of Navier-Stokes boundary-layer computations, while maintaining the robustness of the scalar artificial dissipation scheme with regard to shock capturing. An improved method is presented to define the turbulence length scales in the Baldwin-Lomax and Johnson-King turbulence models. The flow solver allows for multi-block grids which are only C^0 -continuous at block interfaces or even only partly continuous, thus simplifying the grid generation task. It is stressed that, for industrial applications, not only a (multi-block) flow solver, but a complete flow-simulation system must be available, including efficient and robust methods for aerodynamic geometry processing, grid generation, and postprocessing. Results are presented which show the applicability of the flow-simulation system for industrial purposes.

1 INTRODUCTION

In the past 10 years, progress in computational algorithms, numerical grid generation, and computing power has made it possible to solve the Navier-Stokes equations for flows around complex configurations of engineering interest. In particular, it has become feasible to compute compressible, turbulent flows around complete aircraft including the aerodynamic effects of propulsion systems. In order for industry to apply such numerical simulations in a routine fashion, specifically during the design process of aircraft, it is important that the employed means for flow computations, including grid generation, are robust and efficient from industry point of view.

At NLR a Navier-Stokes flow-simulation system, called ENFLOW, based on multi-block structured grids has been developed [5]. This is a collection of CFD (Computational Fluid Dynamics) programs for the computation of flows around complex aerospace configurations based on the Navier-Stokes equations. In order for such a system to be useful for industry, it should have full CFD functionality, thus including programs

for aerodynamic geometry processing, grid generation, flow visualization, and postprocessing. Only then numerically accurate computation results can be efficiently produced at acceptable investments in man hour and computer costs, and low turn-around times may be realized.

In order to provide this full CFD functionality, in the ENFLOW system, the following tools are available (see figure 1):

- the domain modeller ENDOMO, for the subdivision of flow domains around complex configurations into simple subdomains called blocks (block decomposition),
- the grid generator ENGRID, for the generation of grids in edges and faces of blocks, and in the blocks themselves, using algebraic and elliptic methods [24, 25],
- the flow solver ENSOLV, for the solution of the Euler and the thin-layer Navier-Stokes equations in arbitrary multi-block domains,
- the grid adaptor ENADAP, currently being implemented, for the adaption of grids through grid-point movement, in order to improve the accuracy of computational results [8, 9], and
- several flow visualization codes.

Recently, the ENFLOW system has been used by industry as a major flow-analysis tool for CFD analysis of wing-body configurations, and for the aerodynamic integration of propulsion systems with transport-type aircraft.

The total turn-around time of the flow simulation for a new complete aircraft configuration, including the construction of a high-quality, Navier-Stokes multi-block grid, is today of the order of three weeks. However, frequently a total turn-around time of one or a few days may be realized, specifically when computations have to be performed for a well-known topology, or after a moderate geometry modification, which often occurs during aerodynamic design processes. The actual flow computation needs only a computation time of three to five hours (for 1 to 2 million grid cells) on the NLR NEC SX3 supercomputer. These figures concerning turn-around times should be contrasted with those of about five to seven years ago, when multi-block grid generation around complex configurations starting from scratch required three to six man months [4].

¹ National Aerospace Laboratory NLR, P.O. Box 90502, 1006 BM Amsterdam, the Netherlands

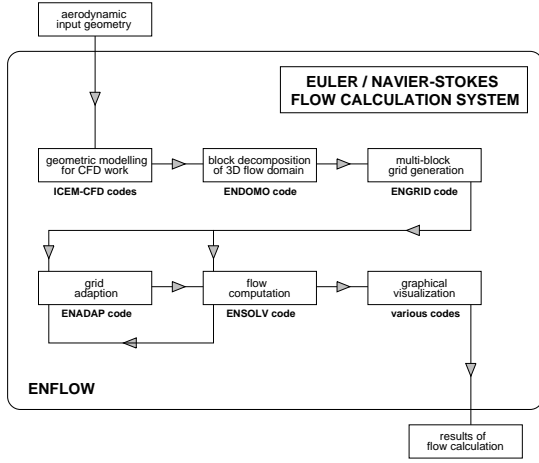


Figure 1. The ENFLOW system

The following sections will give a description of the flow solver ENSOLV, and present computational results obtained with the complete flow-simulation system ENFLOW.

2 CONTINUOUS MODEL

Consider as independent variables the time $t \in [0, \infty)$, and the Cartesian coordinates $\vec{x} = (x, y, z)^T$ with $\vec{x} \in D \subset \mathbb{R}^3$, where D is the flow domain. The flow domain is divided in a set of non-overlapping blocks, and each block may be described by a curvilinear coordinate system $\vec{\xi} = (\xi, \eta, \zeta)^T \in [0, 1]^3$. Let the basic dependent variables be the density ρ , the momentum vector $\rho \vec{u}$, and the total energy per unit volume ρE . Assuming the η -direction to be the normal direction in thin boundary layers or wakes, the thin-layer Reynolds-averaged Navier-Stokes equations may be written as

$$J \frac{\partial U}{\partial t} + \frac{\partial F_\xi^c}{\partial \xi} + \frac{\partial F_\eta^c}{\partial \eta} + \frac{\partial F_\zeta^c}{\partial \zeta} = \frac{\partial F_\eta^d}{\partial \eta}, \quad (1)$$

with $J = \det(d\vec{x}/d\vec{\xi})$, and with U the flow-state vector given by

$$U = \begin{pmatrix} \rho \\ \rho \vec{u} \\ \rho E \end{pmatrix}. \quad (2)$$

The convective flux vector F_η^c and the dissipative flux vector F_η^d are given by

$$F_\eta^c = \begin{pmatrix} \rho u_A \\ \rho \vec{u} u_A + p \vec{A} \\ (\rho E + p) u_A \end{pmatrix}, \quad F_\eta^d = \begin{pmatrix} 0 \\ \vec{\tau}^\eta \\ \vec{u} \cdot \vec{\tau}^\eta - Q^\eta \end{pmatrix} \|\vec{A}\|, \quad (3)$$

with $\vec{A} = J \nabla \eta$ and $u_A = \vec{u} \cdot \vec{A}$. Assuming a perfect gas, the pressure p is given by

$$p = (\gamma - 1) \left(\rho E - \frac{1}{2} \rho \|\vec{u}\|^2 \right), \quad (4)$$

with γ the ratio of specific heats. The shear stress vector $\vec{\tau}^\eta$ and the heat flux Q^η are expressed using the laws of Newton

and Fourier for the viscous contributions, and the Boussinesq hypothesis for the Reynolds stresses, while maintaining only the derivatives in the η direction,

$$\vec{\tau}^\eta = \mu_{\text{tot}} \left(\|\nabla \eta\| \frac{\partial \vec{u}}{\partial \eta} + \frac{1}{3} \left(\nabla \eta \cdot \frac{\partial \vec{u}}{\partial \eta} \right) \frac{\nabla \eta}{\|\nabla \eta\|} \right) \quad (5)$$

$$Q^\eta = -k_{\text{tot}} \|\nabla \eta\| \frac{\partial T}{\partial \eta}, \quad (6)$$

with the temperature T given by the perfect gas law, $T = p/(R\rho)$. The total viscosity μ_{tot} , and the total conductivity k_{tot} are given by

$$\mu_{\text{tot}} = \mu + \mu_t, \quad (7)$$

$$k_{\text{tot}} = C_p \left(\frac{\mu}{Pr} + \frac{\mu_t}{Pr_t} \right), \quad (8)$$

with the laminar viscosity μ given by the Sutherland law, and the eddy-viscosity μ_t given by the Baldwin-Lomax (BL) [3], the Cebeci-Smith (CS) [6], or the Johnson-King (JK) turbulence model [16, 13].

3 NUMERICAL MODEL

3.1 Standard scheme

The standard numerical scheme used in ENSOLV consists of the schemes developed by Jameson [12, 11] and Martinelli [18], which may be considered proven technology (e.g. references [19, 21, 26]). The continuous equations (1) are discretized in space by a cell-centred finite-volume scheme:

$$\frac{dU_{i,j,k}}{dt} = -R_{i,j,k}, \quad (9)$$

$$R_{i,j,k} = (D_{i,j,k}^c - D_{i,j,k}^a - D_{i,j,k}^d) / V_{i,j,k}, \quad (10)$$

with $V_{i,j,k}$ the cell volume, and with the indices (i,j,k) indicating cell centres, corresponding to the curvilinear coordinates (ξ, η, ζ) , respectively. The convective flux balance D^c , the artificial dissipative flux balance D^a , and the physical dissipative flux balance D^d each consist of the summation of the corresponding fluxes across the six faces of the grid cell (i,j,k) . The convective and physical dissipative fluxes at a cell face are given by equation (3), with \vec{A} taken equal to the cell-face area vector, with flow variables located at the cell face defined by simple averaging of the cell-centre values, and with first-order derivatives defined by central differencing in computational space.

In the standard scheme, the scalar artificial dissipation of Jameson [12] is used, which is defined by a blending of second-order differences to obtain physically acceptable representations of shock waves and fourth-order differences to damp high-frequency modes. The artificial dissipative flux at a cell face between cells (i,j,k) and $(i,j+1,k)$ is then given by

$$F_{i,j+1/2,k}^a = \lambda_{i,j+1/2,k} (\epsilon^{(2)} \delta^j U - \epsilon^{(4)} \delta_3^j U)_{i,j+1/2,k} \quad (11)$$

with $\lambda = |u_A + c \|\vec{A}\||$ the spectral radius of the convective Jacobian in j direction (multiplied by the cell-face area), and

with $c = (\gamma p / \rho)^{1/2}$ the speed of sound. The expressions for the i and k directions are similar. The factors $\epsilon^{(2)}$ and $\epsilon^{(4)}$ are given by

$$\epsilon_{ij+1/2,k}^{(2)} = \min \left\{ \frac{1}{2}, k^{(2)} \max \{ \nu_{i,j,k}, \nu_{i,j+1,k} \} \right\}, \quad (12)$$

$$\epsilon_{ij+1/2,k}^{(4)} = k^{(4)} \max \left\{ 0, \frac{1}{64} - k^{(s)} \epsilon_{ij+1/2,k}^{(4)} \right\}, \quad (13)$$

with ν the shock sensor,

$$\nu_{i,j,k} = \frac{|p_{ij+1,k} - 2p_{i,j,k} + p_{ij-1,k}|}{p_{ij+1,k} + 2p_{i,j,k} + p_{ij-1,k}}. \quad (14)$$

In the flow solver, the default values for the parameters of the artificial dissipation are $k^{(2)} = 1$, $k^{(4)} = 2$, and $k^{(s)} = 0.5$, which are used for all computations of section 5.

The discrete equations (9) are solved by Runge-Kutta time integration, accelerated by local time stepping, implicit residual averaging, and a multi-grid scheme. In order to obtain a good damping of high-frequency modes on a grid with cells of high aspect ratio, the high-aspect-ratio scaling of the artificial dissipation and the variable-coefficient residual averaging of Martinelli [18] are used. For each stage of the multi-grid scheme (relaxation, restriction, or prolongation), a complete loop over all the blocks is performed. The relaxation consists of performing a complete Runge-Kutta time step for each block, while keeping the flow states in the other blocks frozen.

An important aspect of the flow solver is the fact that it allows for multi-block grids, which are only C^0 -continuous (and not C^1 -continuous) at block interfaces, or even only partly continuous [17]. The former property greatly simplifies the multi-block grid generation task, allowing for the generation of grids in each block independently, once the grids in block faces have been generated. The latter property makes it possible to locally refine the grid in certain blocks by a factor 2 or 4 if this is considered necessary for accuracy reasons, with only a moderate increase of computation time.

3.2 Matrix artificial dissipation

The standard Jameson-type central differencing scheme with scalar artificial dissipation is generally found to provide rather poor numerical accuracy in boundary layers, e.g. [2, 20, 28], unless very fine grids are used in normal direction, which is often not feasible for industrial applications. To improve the accuracy, the matrix dissipation of Swanson-Turkel [27, 28] may be used. Since the main interest is to improve the accuracy in boundary layers, a modification is applied to the matrix model. This modification essentially consists of applying the matrix dissipation only in normal direction, while in tangential directions the standard scalar dissipation is used. Thus, the basic Jameson shock-capturing scheme can be retained, which provides robustness in particular with regard to shock capturing, while shock resolution may be improved through grid adaptation. Furthermore, this modified matrix dissipation model requires no significant increase in computation time compared to the scalar model.

In the standard matrix dissipation model of Swanson and Turkel, the artificial dissipative flux is given by

$$F_{ij+1/2,k}^a = |\mathcal{A}|_{ij+1/2,k} (\epsilon^{(2)} \delta^j U - \epsilon^{(4)} \delta_3^j U)_{ij+1/2,k} \quad (15)$$

with \mathcal{A} the Jacobian matrix of the convective flux in j direction, and with similar expressions for the i and k directions. Let Λ be the diagonal matrix with the eigenvalues of \mathcal{A} along its diagonal,

$$\Lambda = \text{diag}(\lambda_1, \lambda_1, \lambda_1, \lambda_4, \lambda_5), \quad (16)$$

$$\lambda_1 = u_A, \quad (17)$$

$$\lambda_4 = u_A + c \|\vec{A}\|, \quad (18)$$

$$\lambda_5 = u_A - c \|\vec{A}\|, \quad (19)$$

Let the matrix \mathcal{Q} have the eigenvectors of \mathcal{A} as its column vectors. Then, the absolute value of the Jacobian is defined by taking the absolute value of its eigenvalues,

$$|\mathcal{A}| = \mathcal{Q} |\Lambda| \mathcal{Q}^{-1}, \quad (20)$$

where the matrix $|\Lambda|$ is defined by taking the absolute value of the elements of Λ .

In order to avoid that the eigenvalues can become zero (which is needed in order to satisfy the entropy condition), a lower bound is defined using the spectral radius λ , so that the diagonal elements of $|\Lambda|$ become

$$\tilde{\lambda}_1 = \max \{ |\lambda_1|, \epsilon^L \lambda \}, \quad (21)$$

$$\tilde{\lambda}_4 = \max \{ |\lambda_4|, \epsilon^N \lambda \}, \quad (22)$$

$$\tilde{\lambda}_5 = \max \{ |\lambda_5|, \epsilon^N \lambda \}. \quad (23)$$

Swanson and Turkel [27] at first chose ϵ^L and ϵ^N to be equal to 0.25. This choice, together with a necessary modification of the shock sensor of equation (14), resulted in an improved shock resolution.

However, to improve the accuracy in boundary layers, Swanson and Turkel found it necessary to take ϵ^L equal to 0.01 for the j direction [28]. In this way, the amount of artificial diffusion in the normal direction is strongly reduced for the entropy and shear waves, so that no interference occurs with the physical dissipation. This is specifically the case in the lower region of the boundary layer where λ_1 tends to zero. Sufficient damping of the high-frequency modes in normal direction is provided here by the physical dissipative terms. In practice, convergence is not affected with this choice for ϵ^L , as shown in section 5.

We choose to implement a reduced form of the matrix dissipation model, with as main purpose the reduction of the artificial dissipation for the normal direction in boundary layers and wakes. For the i and k directions, the two factors ϵ^L and ϵ^N are set to one, or, similarly, the scalar dissipation model is applied for these directions (which is computationally more efficient). For the j direction the two factors are set as

$$\epsilon^L = 0.01, \quad (24)$$

$$\epsilon^N = 1. \quad (25)$$

Taking ε^N equal to one, implies that $\tilde{\lambda}_4$ and $\tilde{\lambda}_5$ are equal to the spectral radius λ , so that the standard Jameson shock capturing scheme can be used. Thus, the factors $\varepsilon^{(2)}$ and $\varepsilon^{(4)}$ are defined in the same way as in the scalar model (equations (12) and (13)).

Because of the choice $\varepsilon^N = I$, the final expression for $|\mathcal{A}|$ is also simplified with respect to the standard matrix model, giving a further reduction of the computational effort:

$$|\mathcal{A}| = \tilde{\lambda}_I \mathcal{I} + (\lambda - \tilde{\lambda}_I) \left(\frac{\gamma - 1}{c^2} AC^T - \frac{1}{\|\vec{A}\|^2} BD^T \right), \quad (26)$$

with \mathcal{I} the unit 5x5 matrix, and with the column vectors A , B , C , and D given by

$$A = \begin{pmatrix} I \\ \vec{u} \\ H \end{pmatrix}, \quad B = \begin{pmatrix} 0 \\ \vec{A} \\ u_A \end{pmatrix}, \quad (27)$$

$$C = \begin{pmatrix} \frac{1}{2} \|\vec{u}\|^2 \\ -\vec{u} \\ I \end{pmatrix}, \quad D = \begin{pmatrix} u_A \\ -\vec{A} \\ 0 \end{pmatrix}, \quad (28)$$

in which $H = E + p/\rho$ is the total enthalpy.

4 TURBULENCE MODELLING ASPECTS

A critical aspect of the flow solver with respect to robustness was found to be the implementation of turbulence models. A straightforward implementation in a 3D flow solver of standard algebraic turbulence models, such as the BL and the JK models, usually does not lead to satisfactory results.

In both turbulence models, the location of maxima of functions in boundary-layer normal direction must be determined, while such a location is, in general, not uniquely defined. In the BL model [3], the length scale n_{\max} is required, which is the location of the maximum f_{\max} of the function $f = n\omega D_d$, with n the distance to the solid wall, ω the vorticity magnitude, and D_d the Van Driest damping term. Straightforward computation of this location often leads to a break down of convergence, in particular when there are two local maxima with values close to each other. For a robust computation of this length scale, the following integral formulation is used:

$$n_{\max} = \int_0^\delta \left(\frac{f}{f_{\max}} \right)^q n \, dn \quad / \quad \int_0^\delta \left(\frac{f}{f_{\max}} \right)^q \, dn, \quad (29)$$

with δ (a rough estimate of) the boundary-layer thickness. From figure 2 it may be seen that with a value of $q = 8$, the correct location of the maximum is obtained, when a unique maximum exists. The JK model also employs a length scale n_m , which is the location of the maximum Reynolds shear stress. This length scale may be computed by the same integral formulation.

The BL model is known to give unsatisfactory results for flows with strong adverse pressure gradients (including shock-induced separation). For these type of flows, it has been shown

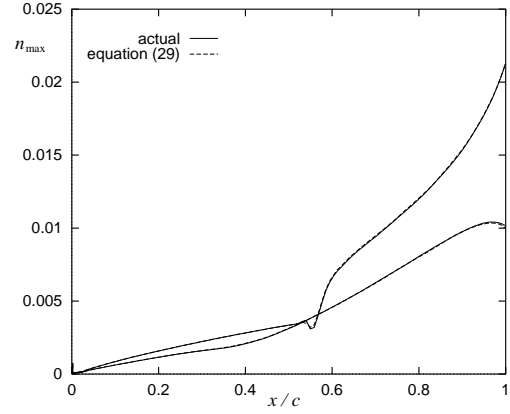


Figure 2. Value of n_{\max} for RAE2822 profile, case 9

that the JK model can give significant improvements (e.g. references [10, 1, 22]). The JK model implemented in ENSOLV includes the improvements of Johnson and Coakley [15]. Furthermore, for the outer viscosity the original Clauser-type formulation is used (in stead of the BL formulation as done by Abid et.al. [1]) as suggested by Johnson [14].

For the JK model, the extension to 3D is not trivial. In 2D, the JK model includes an ordinary differential equation (ODE) for the maximum Reynolds shear stress τ_m^R . For the extension towards 3D, this ODE is often replaced by a 3D partial differential equation (PDE) [1]. However, the form of this 3D PDE is not well-defined in the literature. We employ for 3D flows the following 2D PDE along solid walls:

$$\frac{\partial g}{\partial t} + (\vec{u}_m \cdot \nabla \xi) \frac{\partial g}{\partial \xi} + (\vec{u}_m \cdot \nabla \zeta) \frac{\partial g}{\partial \zeta} = RHS, \quad (30)$$

with the variable $g = \sqrt{\tau_m^R / \rho_m}$, with the subscript m indicating the location n_m , and with ξ and ζ the curvilinear coordinates along the solid wall.

This PDE has a non-conservative form and therefore is discretized by a finite differencing scheme in stead of a finite volume scheme. A second-order fully upwind scheme is employed, to account for a proper numerical treatment of regions of influence and dependence near discontinuities in flow solutions of this PDE. Such discontinuities may be present at attachment and separation lines. An example is strong separation effects near a wing tip, where vortex sheets and/or vortices leave the surface.

The discrete equation for the second-order fully upwind scheme is given by

$$\frac{dg_{s,t}}{dt} = -R_{s,t}^{JK}, \quad (31)$$

$$R_{s,t}^{JK} = Q_{s,t}^{c\xi} + Q_{s,t}^{a\xi} + Q_{s,t}^{c\zeta} + Q_{s,t}^{a\zeta} - RHS_{s,t}, \quad (32)$$

with the indices (s,t) indicating cell centres on the solid wall, and corresponding to the curvilinear coordinates (ξ, ζ) , respectively. The convective and artificial dissipative terms are given by

$$Q_{s,t}^{c\xi} = \lambda_{s,t}^\xi (g_{s+1,t} - g_{s-1,t} - \frac{1}{4}(g_{s+2,t} - g_{s-2,t})), \quad (33)$$

$$Q_{s,t}^{d\xi} = \frac{1}{\tau} |\lambda_{s,t}^\xi| \delta_4^s g, \quad (34)$$

with $\lambda^\xi = \vec{u}_m \cdot (\nabla \xi)$.

The discrete equations (31) are solved by a 5-stage Runge-Kutta scheme, particularly tuned for the fully-upwind scheme [29]. For each multi-grid cycle of the main flow equations, a time step is performed. In practice, this solution method does not deteriorate the multi-grid convergence, mainly because the boundary-layer normal direction (with small mesh sizes in this direction) is not included in the 2D PDE of equation (30).

It should be pointed out that the JK model is an intricate model (including also four implicit algebraic relations to solve) containing many detailed problems to tackle in order to make it applicable in a routine fashion. Only the two main measures we have taken have been described here. Even though these measures have improved the robustness of the implementation of the model in 3D, still the equations may not always converge fully to steady state. In fact, one may state that algebraic models are usually strongly depended on typical boundary-layer quantities and thus cannot be expected to always work for general 3D configurations. Presently, work is being done on the implementation of more general turbulence model, such as two-equation models.

5 RESULTS

The improvement of the boundary-layer resolution using the modified matrix dissipation scheme is shown for the RAE2822 airfoil, case 9 ($M_\infty = 0.73$, $Re_\infty = 6.5 \cdot 10^6$, $\alpha = 2.8^\circ$) [7]. Figures 3 and 4 show the skin-friction coefficient and the displacement thickness along the airfoil on a fine grid (528×96 grid cells) with the matrix model, and on the corresponding medium grid (mesh sizes doubled) with the scalar and the matrix model. With the matrix model, the solution on the

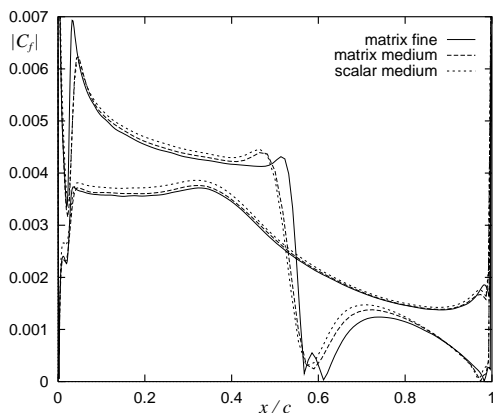


Figure 3. Skin friction for RAE2822, case 9

medium grid is significantly closer to the fine-grid solution (in particular on the lower side) than with the scalar model. As can be seen from figure 5 the improved boundary-layer resolution has been obtained with no degradation of convergence

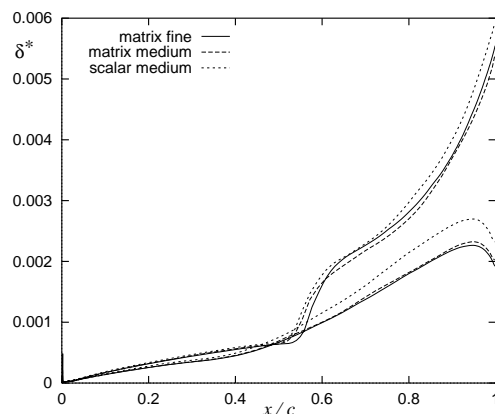


Figure 4. Displacement thickness for RAE2822, case 9

speed, and furthermore with no significant increase of computation time (less than 1%). The main difference between the

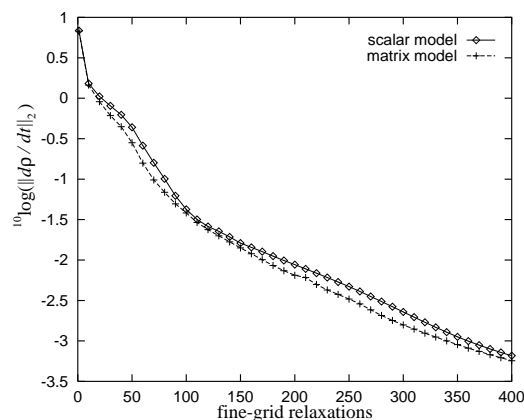


Figure 5. Convergence history for RAE2822, case 9

medium-grid and fine-grid solutions with the matrix model is located around the shock. The shock resolution may be improved by using the standard matrix model of Swanson-Turkel at the cost of a moderate loss of convergence speed and an increase of computation time (in the order of 15%) [28]. The shock resolution may also be improved using grid adaptation based on grid-point movement [8, 9].

The application of the JK model in 3D is shown for two cases: the ONERA M6 wing and the Aerospatiale AS28G wing/body configuration. For the ONERA M6 wing a 4-block CO-type grid with a total of 0.8 million grid cells has been used. The test case for the ONERA M6 wing ($M_\infty = 0.8447$, $Re_\infty = 11.78 \cdot 10^6$, $\alpha = 5.06^\circ$) has strong shock-induced separation. Figure 6 shows that the JK model results in a better pressure distribution than the CS model (compared to the experiment [23]) consistent with references [1, 22].

The ENFLOW system has been used intensively by industry for computations around wing/body/pylon/nacelle configurations, for which the JK model was found to give satis-

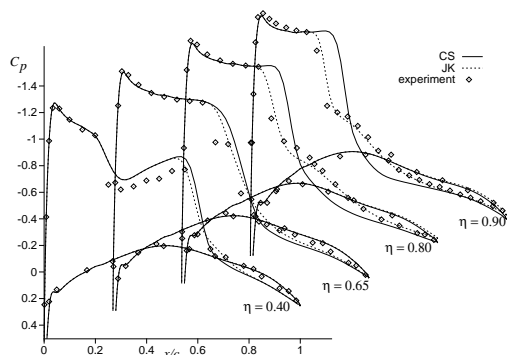


Figure 6. Pressure coefficient for ONERA M6 wing

factory results. As an illustration, preliminary results for the Aerospatiale AS28G wing/body configuration ($M_\infty = 0.80$, $Re_\infty = 10.5 \cdot 10^6$, $\alpha = 2.20^\circ$) have been included (figure 7). A 32-blocks grid has been used with a total of 1.2 million grid

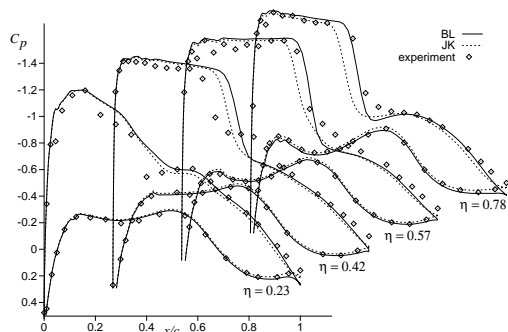


Figure 7. Pressure coefficient for AS28G wing/body

cells, and with the no-slip condition only applied on the wing. For this case, besides the shock position, the JK model also has effect on the pressure distribution on the aft part of the wing. Comparison with the experimental results is not fully satisfactory, in particular with respect to the shock position. However, uncertainties exist about the geometry definition (smoothed out kink) and wind-tunnel conditions, so that an explanation of the differences cannot (yet) be given. The convergence history of figure 8 shows comparable convergence speeds for the BL and JK turbulence models. The JK model generally requires an increase of the computation time per iteration of the order of 10%, compared to the BL and CS models.

The applicability of the complete ENFLOW system to complex configurations is finally shown for an AS28G wing/body/nacelle configuration (without pylon). The complete flow simulation, including the generation of a 101-block grid, could be performed within three weeks. An impression of the grid is given in figure 9. Recomputation of the flow after repositioning of the nacelle may be performed within

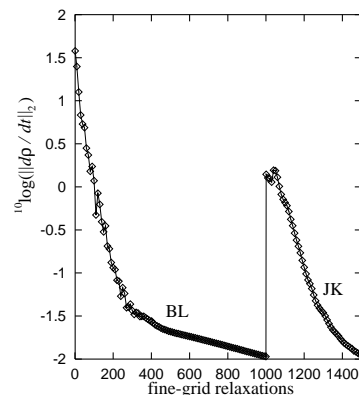


Figure 8. Convergence history for AS28G wing/body

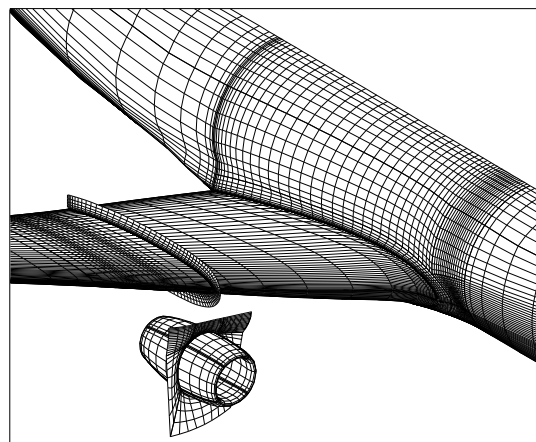


Figure 9. Impression of grid around AS28G wing/body/nacelle

one or a few days. Figure 10 compares the computational results for the wing/body and wing/body/nacelle configurations with the experimental results for the wing/body and the wing/body/pylon/nacelle configurations. The computations were performed with the BL model and on medium grid levels (0.15 and 0.28 million grid cells). The modification of the pressure distribution on the lower side, as well as the forward shock movement, are consistent between the computational and experimental results, although there is still an inconsistency in the actual shock position (as for the wing/body case).

6 CONCLUDING REMARKS

A robust multi-block flow solver for the thin-layer Reynolds-averaged Navier-Stokes equations has been presented. It has been shown that with a modified form of the matrix artificial dissipation model the numerical accuracy in boundary layers may be improved, while maintaining the standard robust shock capturing scheme, and without a significant increase of computation time. Implementation aspects of algebraic turbulence models have been discussed that improve the robustness

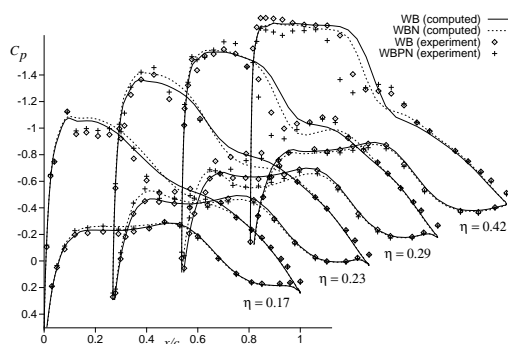


Figure 10. Pressure coefficients for AS28G wing/body and wing/body/nacelle

of the solver. Finally, it has been shown that industrial numerical flow simulations may be performed efficiently with the flow-simulation system ENFLOW.

ACKNOWLEDGEMENTS

This work has been carried out under a contract awarded by the Netherlands Agency for Aerospace Programs, NIVR, contract number 01105N.

REFERENCES

- [1] R. Abid, V.N. Vatsa, D.A. Johnson, and B.W. Wedan, 'Prediction of separated transonic wing flows with a non-equilibrium algebraic model'. AIAA-89-0558, 1989.
- [2] S.R. Allmaras, 'Contamination of laminar boundary layers by artificial dissipation in Navier-Stokes solutions'. Conference on Numerical Methods in Fluid Dynamics, April 7-10 1992.
- [3] B.S. Baldwin and H. Lomax, 'Thin-layer approximation and algebraic model for separated turbulent flows'. AIAA-78-257, 1978.
- [4] J.W. Boerstoel, J.M.J.W. Jacobs, A. Kassies, A. Amendola, R. Tognaccini, and P.L. Vitagliano, 'Design and testing of a multiblock grid-generation procedure for aircraft design and research'. Presented at 64th meeting of the AGARD Fluid Dynamics Panel on Applications of Mesh Generation to Complex 3D Configurations, (NLR TP 89146 U), May 1989.
- [5] J.W. Boerstoel, S.P. Spekreijse, and P.L. Vitagliano, 'The design of a system of codes for industrial calculations of flows around aircraft and other complex aerodynamic configurations'. AIAA-92-2919, 1992.
- [6] T. Cebeci and A.M.O. Smith, *Analysis of turbulent boundary layers*, Academic Press, New York, 1974.
- [7] P. Cook, M. McDonald, and M. Firmin, 'Airfoil RAE 2822 - pressure distributions and boundary layer wake measurements'. AGARD AR-138, p. A6, 1979.
- [8] R. Hagmeijer, 'Grid adaption based on modified anisotropic diffusion equations formulated in the parametric domain', *Journal of Computational Physics*, **115**, 169-183, (1994).
- [9] R. Hagmeijer and J.C. Kok, 'Adaptive 3D single-block structured grids for the computation of viscous flows around wings'. Presented at 5th International Conference on Numerical Grid Generation in Computational Fluid Dynamics and Related Fields, 1995.
- [10] T.L. Holst, 'Viscous transonic airfoil workshop compendium of results'. AIAA-87-1460, 1987.
- [11] A. Jameson, 'Multigrid algorithms for compressible flow calculations'. Report 1743, Dept. of Mech. and Aerosp. Eng., Princeton University.
- [12] A. Jameson, W. Schmidt, and E. Turkel, 'Numerical solution of the Euler equations by finite volume methods using Runge-Kutta time-stepping schemes'. AIAA-81-1259, 1981.
- [13] D.A. Johnson, 'Predictions of transonic separated flow with an eddy-viscosity/reynolds-shear-stress closure model'. AIAA-85-1683, 1985.
- [14] D.A. Johnson, 'Nonequilibrium algebraic turbulence modeling considerations for transonic airfoils and wings'. AIAA-92-0026, 1992.
- [15] D.A. Johnson and T.J. Coakley, 'Improvements to a non-equilibrium algebraic turbulence model', *AIAA Journal*, **28**, 2000-2003, (1990).
- [16] D.A. Johnson and L.S. King, 'A new turbulence closure model for boundary layer flows with strong adverse pressure gradients and separation'. AIAA-84-0175, 1984.
- [17] A. Kassies and R. Tognaccini, 'Boundary conditions for Euler equations at internal block faces of multi-block domains using local grid refinement'. AIAA-90-1590, 1990.
- [18] L. Martinelli, *Calculations of Viscous Flows with a Multigrid Method*, PhD dissertation, Princeton University, 1987.
- [19] L. Martinelli and A. Jameson, 'Validation of a multigrid method for the Reynolds averaged equations'. AIAA-88-0414, 1988.
- [20] R. Ramakrishnan, V. Vatsa, J. Otto, and A. Kumar, 'A detailed study of mean-flow solutions for stability analysis of transitional flows'. AIAA 93-3052, 1993.
- [21] C.-C. Rossow, 'Efficient computation of inviscid flow fields around complex configurations using a multi-block multigrid method'. Fifth Copper Mountain Conference on Multigrid Methods, March 31 - April 5 1991.
- [22] C.L. Rumsey and V.N. Vatsa, 'A comparison of the predictive capabilities of several turbulence models using upwind and central-difference computer codes'. AIAA-93-0192, 1992.
- [23] V. Schmitt and F. Charpin, 'Pressure distributions on the ON-ERA M6 wing at transonic Mach numbers'. AGARD AR-138, p. B1, 1979.
- [24] S.P. Spekreijse, 'Elliptic grid generation based on Laplace equations and algebraic transformations', *Journal of Computational Physics*, **118**, 38-61, (1995).
- [25] S.P. Spekreijse, G.H. Nijhuis, and J.W. Boerstoel, 'Elliptic surface grid generation on minimal and parameterized surfaces'. Presented at NASA Workshop on Surface Modeling, Grid Generation, and Related Issues in CFD Solutions, (NLR TP 95122 U), May 1995.
- [26] R.C. Swanson and R. Radespiel, 'Cell centered and cell vertex multigrid schemes for the Navier-Stokes equations', *AIAA Journal*, **29**, 697-703, (1991).
- [27] R.C. Swanson and E. Turkel, 'On central-difference and upwind schemes', *Journal of Computational Physics*, **101**, 292-306, (1992).
- [28] R.C. Swanson and E. Turkel, 'Aspects of a high-resolution scheme for the Navier-Stokes equations'. AIAA-93-3372-CP, 1993.
- [29] B. van Leer, C-H. Tai, and K.G. Powell, 'Design of optimally smoothing multi-stage schemes for the Euler equations'. AIAA-89-1933-CP, 1989.